ARTICLES

Journal of Semiconductors
(2020) 41, 122502
doi: 10.1088/1674-4926/41/12/122502

An antiferromagnetic two-dimensional material: Chromium diiodides monolayer

Jingjing Zhang[1], Jin Yang[1], Liangzhong Lin[2], and JiaJi Zhu[1, †]

[1]School of Science and Laboratory of Quantum Information Technology, Chongqing University of Posts and Telecommunications, Chongqing 400061, China

[2]School of Information Engineering, Zhongshan Polytechnic, Zhongshan 528400, China

Abstract: The two-dimensional (2D) ferromagnetic materials and the related van der Waals homostructures have attracted considerable interest, while the 2D antiferromagnetic material has not yet been reported. Based on first-principles calculations, we investigate both electronic structures and magnetic orderings of bulk and monolayer of chromium diiodides (CrI_2). We demonstrate a counter-intuitive fact that the ground state of the free-standing monolayer of CrI_2 is antiferromagnetic though the bulk possesses macroscopic ferromagnetic ordering. The interlayer interaction remains antiferromagnetic up to few-layer scenarios. The unique feature of CrI_2 makes it an ideal workbench to investigate the relation between magnetic couplings and interlayer van der Waals interactions, and may offer an opportunity to 2D antiferromagnetic spintronic devices.

Key words: first-principles calculation; chromium diiodide; two-dimensional materials; two-dimensional antiferromagnet;

Citation: J J Zhang, J Yang, L Z Lin, and J J Zhu, An antiferromagnetic two-dimensional material: Chromium diiodides monolayer[J]. *J. Semicond.*, 2020, 41(12), 122502. http://doi.org/10.1088/1674-4926/41/12/122502

1. Introduction

Magnetism, which is the macroscopic spin ordering in spatial space, has attracted many studies in the recently flourishing research of two-dimensional (2D) materials[1–5]. In the cases of one- or two-dimension, magnetism tends to be destroyed by any thermal fluctuation in isotropic spin systems at any non-zero temperature, and this statement was recognized as the Mermin-Wagner theorem[6]. In recent years, thanks to the rapid progress in 2D materials[7, 8], scientists have managed to fabricate ultra-thin candidates hosting detectable ferromagnetic orderings[9, 10] because the 2D ferromagnetic ordering could provide ideal platforms for understanding the low-dimensional magnetism[11] and provide opportunities for realizing atomically thin, flexible magneto-optic or magnetoelectric devices.

Pioneering efforts have been made in exfoliation of monolayer and few-layers of magnetic layered bulk materials, such as $NiPS_3$[12], $FePS_3$[13], and $CrSiTe_3$[14]. However, the macroscopic magnetic orders are only observed in thin films. The atomically-thick CrI_3[9] and $Cr_2Ge_2Te_6$[10] down to the monolayer and bilayer limit have been successfully fabricated and corresponding experiments have demonstrated the existence of the intrinsic ferromagnetism (FM). The numbers of 2D ferromagnets, such as Fe_3GeTe_2[15], 1T-VSe_2[16], $MnSe_x$[17], and so on, then mushroomed. All monolayer 2D ferromagnetic materials display significant magnetic anisotropy, which opens a magnon excitation gap and lifts the Wagner-Mermin criteria to finite T_c by suppressing thermal fluctuations[18, 19]. Discoveries of monolayer ferromagnets not only enriched the family of 2D materials but also provide exciting possibilities for device functionalities by the seamless integration of 2D ferromagnets with other nonmagnetic 2D materials via the van der Waals (vdW) heterostructure[20]. Compared to the rapid progress in 2D ferromagnets, the research of low-dimensional antiferromagnets only appear as interlayer couplings in vdW ferromagnetic multilayers[9, 21] but are rarely reported in monolayer limit. This scenario requires precise control of the number of multilayers because even numbers of layers lead to FM and only odd numbers of layers exhibit antiferromagnetism (AFM). Note that most of the discovered magnetic 2D materials possessing ferromagnetic orderings in monolayers show no magnetism in bulk because the interlayer coupling between magnetic monolayers is antiferromagnetic.

2. Methods

In this paper, we investigate both electronic structures and magnetic orderings of bulk and monolayer forms of chromium diiodides, based on the state-of-the-art first-principles calculations[22, 23]. The first-principles calculations are performed by using the Vienna *ab initio* simulation package (VASP)[24–26] within the generalized Kohn-Sham scheme. The projector augmented-wave (PAW)[27, 28] pseudopotentials are adopted, and the kinetic cut-off energy is set to be 680 eV for wave-function expansions, a Γ-centred K-point grid is densely sampled by sums over $15 \times 15 \times 1$. To determine the magnetic ordering of the ground states, the constrained spin-polarized band structures calculations are performed.

3. Results and discussion

3.1. Bulk CrI_2

The bulk CrI_2 crystallizes in the P63mc space group and is consisting of two CrI_2 monolayers in AB stacking. The crystal structure of bulk CrI_2 is shown in Fig. 1(a), the chromium and

Correspondence to: J J Zhu, zhujj@cqupt.edu.cn
Received 17 APRIL 2020; Revised 7 MAY 2020.

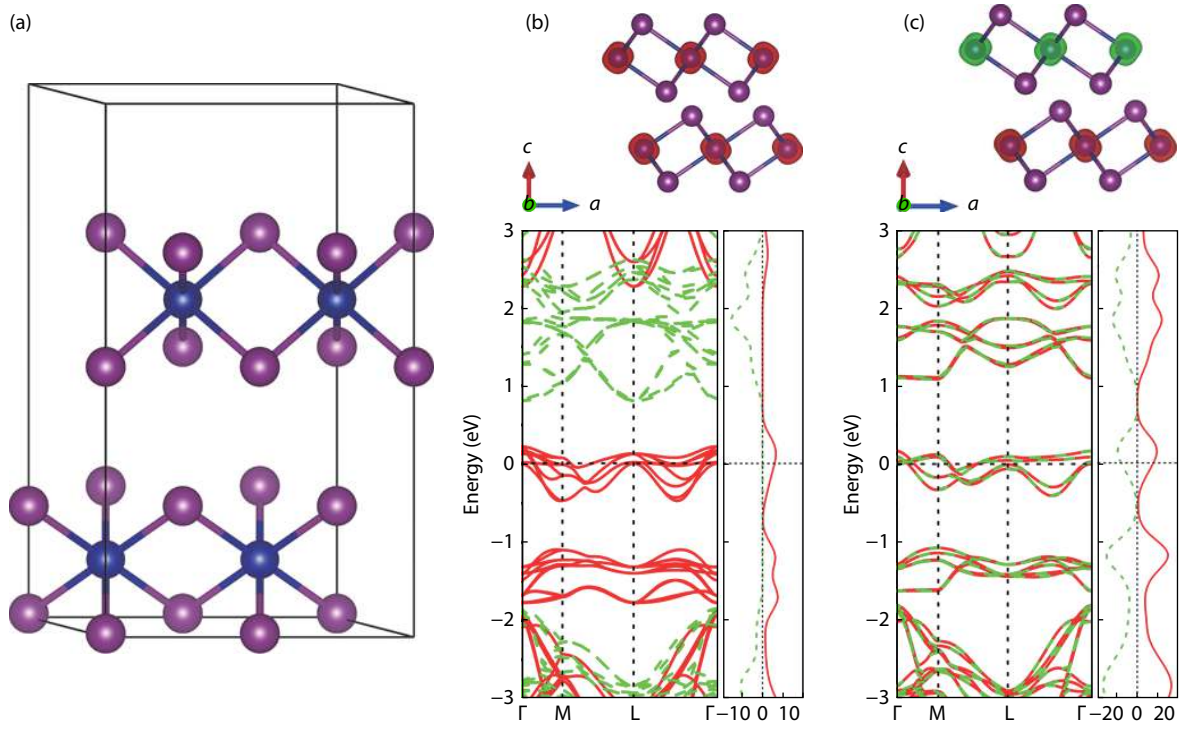

Fig. 1. (Color online) (a) Crystal structure of bulk CrI_2, and spin-polarized band structure and spin spatial distribution of (b) ferromagnetic and (c) antiferromagnetic orderings.

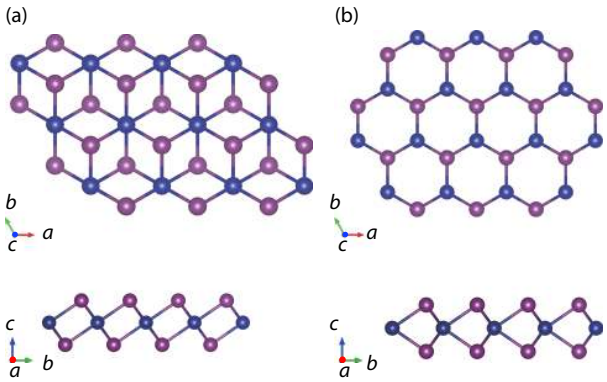

Fig. 2. (Color online) (a) 1T and (b) 2H phases of CrI_2 monolayers. The chromium and iodine atoms are illustrated with blue and purple spheres, respectively.

iodine atoms are displayed with blue and purple spheres, respectively. The spin-polarized band structures of bulk CrI_2 is shown in Fig. 1(b) (antiferromagnetic) and Fig. 1(c) (ferromagnetic), to compare the total energy difference between ferromagnetic and antiferromagnetic orderings, a $2 \times 1 \times 1$ supercell is used, and the band dispersions of spin majority and spin minority is indicated by red and green lines. The corresponding spin spatial distribution is illustrated in inserts of Figs. 1(b) and 1(c)) with the same color-coding. Since the total energy difference between ferromagnetic and antiferromagentic states is 20 meV/unit cell, one can find out that, bulk CrI_2 take a ferromagnetic ground state.

3.2. CrI_2 monolayer

CrI_2 monolayer is cleaved from a fully relaxed bulk crystal. Each chromium atom is bonded to six iodine atoms in the monolayer, and all the atoms are arranged in the 1T phase. Noticing the similarity of CrI_2 monolayer to the famous transitional metal dichalcogenide monolayers, it is necessary to consider the 2H phase. The 1T and 2H phases of CrI_2 monolayers are illustrated in Fig. 2.

In Fig. 3, the spin-resolved band structures, the total spin density of states (DOS) and spin spatial distributions of 1T and 2H CrI_2 monolayers are shown. $2 \times 1 \times 1$ supercells are also employed, to determine the magnetic ground states, by performing constrained spin-polarized first-principles calculations. The numerical results for 1T-FM, 1T-AFM, 2H-FM, 2H-AFM are displayed in panels Figs. 3(a)–3(d) accordingly, and the total energies for each configuration are listed in Table 1. One can find from Table 1 the most energy-favored configuration is 1T-AFM, which implies the ground state of monolayer CrI_2 is antiferromagnetic.

Table 1 shows the total energies of the FM state and the AFM state of the 1T phase, where the energy differences between the FM and the AFM states are obtained by performing DFT+U calculations within Dudarev's approach. The U_{eff} (U–J) varies from 1 to 4 eV, and the corresponding total energy differences are of 30 meV, which indicates the AFM state is more energetic favorable.

3.3. CrI_2 bilayer

To investigate the magnetic effect of the interlayer interaction, we construct a CrI_2 bilayer from 1T CrI_2 monolayers, and to clarify the influence of stacking patterns, both AB stacking and AA stacking models are constructed. As shown in Fig. 4, we denote these models, for convenience, as AA-FM, AA-AFM-a, AA-AFM-f, AB-FM, AB-AFM-a and AB-AFM-f, where the appendix a (f) indicates that the intra-layer initial magnetic moment is set antiferromagnetic (ferromagnetic). The interlayer distance between the adjacent chromium layers in equilibrium is obtained by relaxation and reads XX for the AA stacking and XX for the AB stacking, respectively.

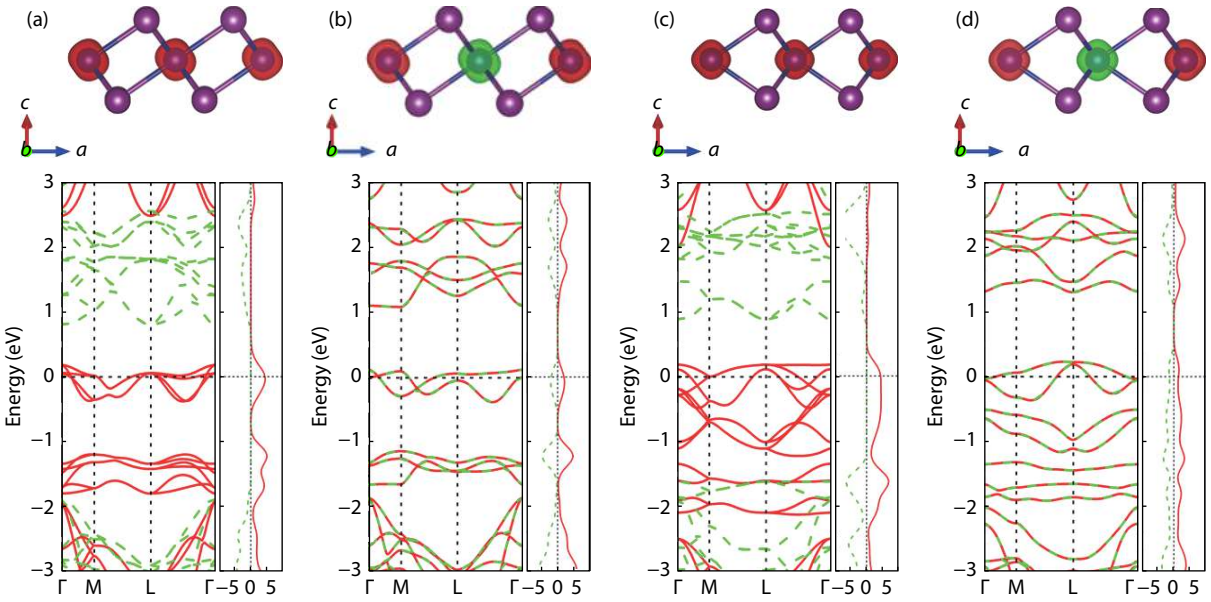

Fig. 3. (Color online) The spin-resolved band structures, total spin density of states (DOS) and spin spatial distributions of (a) 1T-FM, (b) 1T-AFM, (c) 2H-FM, and (d) 2H-AFM.

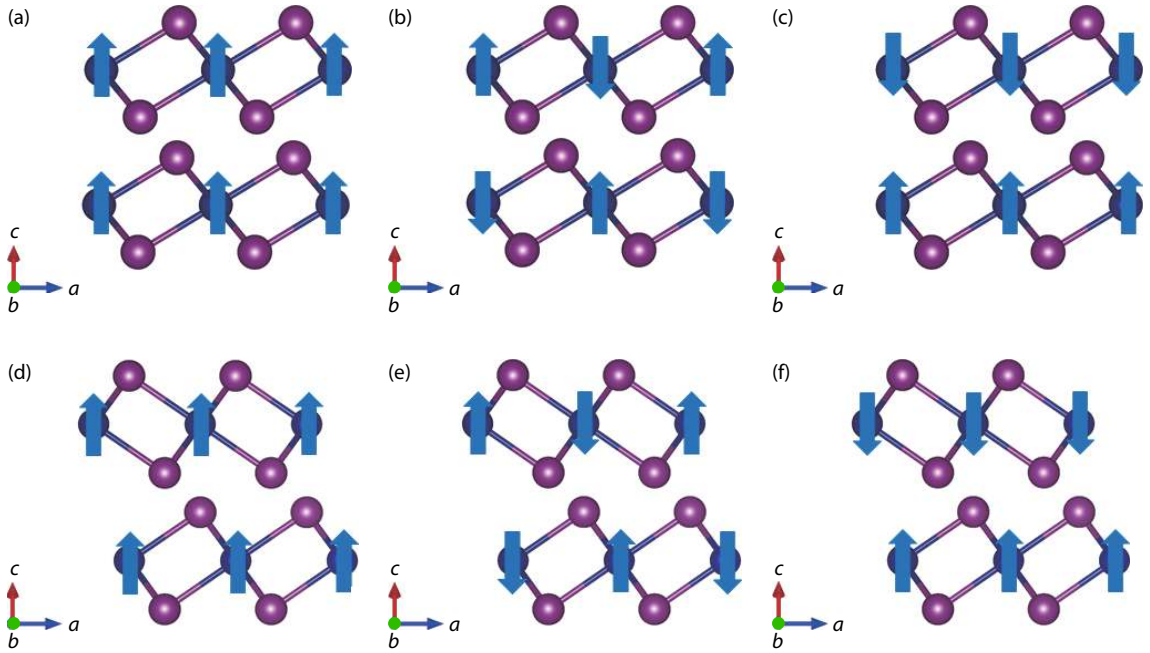

Fig. 4. (Color online) Configurations of the model (a) AA-FM, (b) AA-AFM-a, (c) AA-AFM-f, (d) AB-FM, (e) AB-AFM-a, and (f) AB-AFM-f. The up and down arrows indicate the signs of initial magnetic moments in constrained DFT calculations.

Table 1. The total energies of 1T and 2H phases.

Parameter	FM (eV)	AFM (eV)
1T	−26.464	−26.467
2H	−25.065	−25.148

The spin-resolved band structures, total spin density of states and spin spatial distributions of each CrI_2 bilayers are shown in Fig. 5. The total energies for each configuration are listed in Table 2. From Table 3, one can find the ground states of CrI_2 bilayers are always antiferromagnetic independent of the stacking patterns, which implies the interlayer interaction is still antiferromagnetic in CrI_2 up to few layers.

Table 2. The DFT+U total energies and energy difference for the 1T phase AFM and FM state.

J (eV)		U (eV)		
		2	3	4
0.9	AFM	−25.417	−24.519	−23.560
	FM	−25.361	−24.416	−23.525
	$\lvert\Delta E\rvert$	0.056	0.103	0.035
0.5	AFM	−25.031	−24.092	−23.217
	FM	−24.976	−24.053	−23.184
	$\lvert\Delta E\rvert$	0.055	0.039	0.033
0.1	AFM	−24.679	−23.735	−22.883
	FM	−24.600	−23.699	−22.851
	$\lvert\Delta E\rvert$	0.079	0.036	0.032

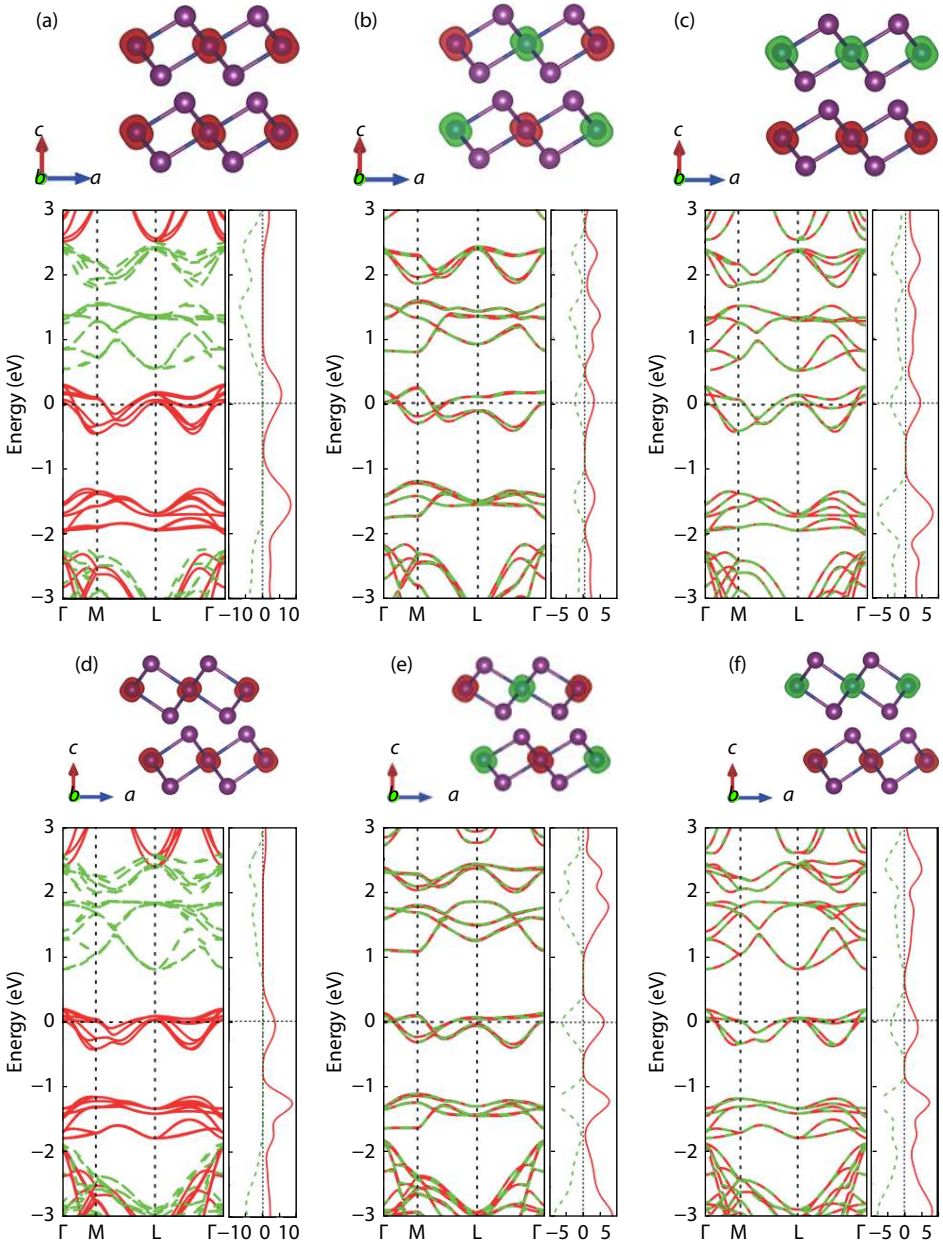

Fig. 5. (Color online) (The spin-resolved band structures, total spin density of states (DOS) and spin spatial distributions of model (a) AA-FM, (b) AA-AFM-a, (c) AA-AFM-f, (d) AB-FM, (e) AB-AFM-a, and (f) AB-AFM-f.

Table 3. AA and AB total energies.

Parameter	FM (eV)	AFM-a (eV)	AFM-f (eV)
AA	−52.277	−52.333	−52.271
AB	−52.890	−52.935	−52.926

4. Conclusion

In summary, we investigate both electronic structures and magnetic orderings of bulk and monolayer forms of chromium diiodides by first-principles calculations and demonstrate that the ground state of a free-standing monolayer of chromium diiodides is antiferromagnetic, even though the bulk possesses macroscopic ferromagnetic ordering. The stable CrI_2 monolayer takes a 1T-phase configuration and the interlayer interaction remains antiferromagnetic up to few-layer scenarios. The robust antiferromagnetic feature makes monolayer or few layers CrI_2 possible blocks to build flexible 2D antiferromagnetic spintronic devices. The questions of why the magnetic structures of monolayer and bulk CrI_2 are opposite and how dependent antiferromagnetic interlayer interaction depend on the layer numbers are still to be answered.

Acknowledgements

This work was supported by the National Natural Science Foundation of China (No. 11404043) and Graduate Research Innovation Project of Chongqing (No. CYS18253).

References

[1] Tokmachev A M, Averyanov D V, Parfenov O E, et al. Emerging two-dimensional ferromagnetism in silicene materials. Nat Commun, 2018, 9, 1672

[2] Shi X Y, Huang Z J, Huttula M, et al. Introducing magnetism into 2D nonmagnetic inorganic layered crystals: A brief review from

first-principles aspects. Crystals, 2018, 8, 24
[3] Tao P, Guo H H, Yang T, et al. Strain-induced magnetism in MoS_2 monolayer with defects. J Appl Phys, 2014, 115, 054305
[4] Kochat V, Apte A, Hachtel J A, et al. Re doping in 2D transition metal dichalcogenides as a new route to tailor structural phases and induced magnetism. Adv Mater, 2017, 29, 1703754
[5] Hallal A, Ibrahim F, Yang H X, et al. Tailoring magnetic insulator proximity effects in graphene: First-principles calculations. 2D Mater, 2017, 4, 025074
[6] Mermin N D, Wagner H. Absence of ferromagnetism or antiferromagnetism in one- or two-dimensional isotropic Heisenberg models. Phys Rev Lett, 1966, 17, 1133
[7] Miao N H, Xu B, Zhu L G, et al. 2D intrinsic ferromagnets from van der Waals antiferromagnets. J Am Chem Soc, 2018, 140, 2417
[8] Lin X, Yang W, Wang K L, et al. Two-dimensional spintronics for low-power electronics. Nat Electron, 2019, 2, 274
[9] Huang B, Clark G, Navarro-Moratalla E, et al. Layer-dependent ferromagnetism in a van der Waals crystal down to the monolayer limit. Nature, 2017, 546, 270
[10] Gong C, Li L, Li Z L, et al. Discovery of intrinsic ferromagnetism in two-dimensional van der Waals crystals. Nature, 2017, 546, 265
[11] Sheng X L, Nikolić B K. Monolayer of the 5d transition metal trichloride $OsCl_3$: A playground for two-dimensional magnetism, room-temperature quantum anomalous Hall effect, and topological phase transitions. Phys Rev B, 2017, 95, 201402
[12] Kuo C T, Neumann M, Balamurugan K, et al. Exfoliation and Raman spectroscopic fingerprint of few-layer $NiPS_3$ van der waals crystals. Sci Rep, 2016, 6, 20904
[13] Zhu W, Gan W, Muhammad Z, et al. Exfoliation of ultrathin $FePS_3$ layers as a promising electrocatalyst for the oxygen evolution reaction. Chem Commun, 2018, 54, 4481
[14] Li X X, Yang J L. $CrXTe_3$ (X = Si, Ge) nanosheets: Two dimensional intrinsic ferromagnetic semiconductors. J Mater Chem C, 2014, 2, 7071
[15] Zhuang H L, Kent P R C, Hennig R G. Strong anisotropy and magnetostriction in the two-dimensional Stoner ferromagnet Fe_3GeTe_2. Phys Rev B, 2016, 93, 134407
[16] Yadav C S, Rastogi A K. Transport and magnetic properties of Fe_xVSe_2 (x = 0–0.33). J Phys: Condens Matter, 2008, 20, 465219
[17] Sun J J, Li C, Chen D, et al. Controlled synthesis of ferromagnetic $MnSe_x$ particles. Chin Phys B, 2016, 25, 107405
[18] Lado J L, Fernández-Rossier J. On the origin of magnetic anisotropy in two dimensional CrI_3. 2D Mater, 2017, 4, 035002
[19] Abramchuk M, Jaszewski S, Metz K R, et al. Controlling magnetic and optical properties of the van der waals crystal $CrCl_{3-x}Br_x$ via mixed halide chemistry. Adv Mater, 2018, 30, 1801325
[20] Gibertini M, Koperski M, Morpurgo A F, et al. Magnetic 2D materials and heterostructures. Nat Nanotechnol, 2019, 14, 408
[21] Gong S J, Gong C, Sun Y Y, et al. Electrically induced 2D half-metallic antiferromagnets and spin field effect transistors. PNAS, 2018, 115, 8511
[22] Hohenberg P, Kohn W. Inhomogeneous electron gas. Phys Rev, 1964, 136, b864
[23] Kohn W, Sham L J. Self-consistent equations including exchange and correlation effects. Phys Rev, 1965, 140, a1133
[24] Kresse G, Hafner J. Ab initio molecular-dynamics simulation of the liquid-metal-amorphous-semiconductor transition in germanium. Phys Rev B, 1994, 49, 14251
[25] Kresse G, Furthmüller J. Efficiency of ab-initio total energy calculations for metals and semiconductors using a plane-wave basis set. Comput Mater Sci, 1996, 6, 15
[26] Kresse G, Furthmüller J. Efficient iterative schemes for ab initio total-energy calculations using a plane-wave basis set. Phys Rev B, 1996, 54, 11169
[27] Blöchl P E. Projector augmented-wave method. Phys Rev B, 1994, 50, 17953
[28] Kresse G, Joubert D. From ultrasoft pseudopotentials to the projector augmented-wave method. Phys Rev B, 1999, 59, 1758